Journal of Computer-Aided Molecular Design (2025) 39:57
https://doi.org/10.1007/s10822-025-00633-0

Molecular dynamics simulations reveal mechanistic insights into aptamer-induced structural rearrangements in viral capsid proteins

Chen Fei Low[1] · Norazli Ghadin[1] · Muhamad Arif Mohamad Jamali[2]

Received: 14 April 2025 / Accepted: 6 July 2025 / Published online: 23 July 2025

Abstract

Macrobrachium rosenbergii nodavirus is a major viral pathogen responsible for white tail disease in giant freshwater prawn aquaculture, leading to significant economic losses. In this study, a truncated DNA aptamer, TrAptm-1 was investigated for its binding properties against both monomeric and trimeric forms of the MrNV capsid proteins. Molecular dynamics simulations coupled with MM/PBSA binding free energy calculations revealed that TrAptm-1 exhibited a higher binding affinity to the trimeric capsid protein (-153.95 ± 6.74 kcal/mol) compared to the monomeric form (-120.77 ± 2.46 kcal/mol). TrAptm-1 binding induced significant conformational changes and structural rearrangements in the capsid protein, highlighted the antiviral potential of TrAptm-1 to interfere with the capsid protein self-assembly process. The observed structural changes demonstrated the importance of the oligomeric state in aptamer-capsid protein interactions, emphasizing that extended simulations up-to microseconds are required to capture the slow conformational rearrangements characteristic of large oligomeric protein complexes. These findings provide a molecular basis for the development of aptamer-based antiviral strategies, and the design of biosensor for early detection of MrNV in aquaculture settings.

Keywords Aptamer · Viral capsid protein · Conformational changes · Binding affinity

Introduction

Macrobrachium rosenbergii nodavirus (MrNV) is the causative agent of White Tail Disease (WTD), a severe viral infection that significantly affects the giant freshwater prawn aquaculture. The virus belongs to the Nodaviridae family. It forms non-enveloped, icosahedral virions with a diameter of approximately 27 nm. The viral structural protein composed of a single capsid protein of 43 kDa, which undergoes autocatalytic cleavage to produce a smaller 37 kDa mature protein responsible for viral particle assembly. During infection, MrNV capsid proteins accumulate in the cytoplasm of infected prawn cells, where the capsid protein monomers self-assemble into T = 3 icosahedral particles that encapsidate two positive-sense, single-stranded RNA molecules comprising the viral genome [1]. The abundance of different oligomeric forms of the capsid proteins in infected prawn cells presents a promising target for the development of effective diagnostic and therapeutic strategies for disease detection and treatment. Aptamer-based diagnostic and therapeutic interventions targeting the viral capsid protein has been shown promising in various viral infections [2–5].

Aptamers are short, single-stranded oligonucleotides that can selectively bind to specific molecular targets. Aptamers are selected through Systematic Evolution of Ligands by EXponential enrichment (SELEX), have gained significant attention for their diverse applications in both therapeutics and diagnostics [6–9]. Despite their promising applications, the structural basis of aptamer binding and interaction with target molecules remains a challenging aspect of aptamer-based research. In previous study, SELEX was performed using monomeric recombinant MrNV capsid protein as the target, leading to the identification of a ssDNA aptamer (APT-MrNV-CP-1) [10]. Further optimization of the aptamer-protein binding affinity revealed that the truncation to remove non-essential region of the aptamer further

✉ Chen Fei Low
low@ukm.edu.my

✉ Muhamad Arif Mohamad Jamali
arifjamali@usim.edu.my

[1] Institute of Systems Biology, Universiti Kebangsaan Malaysia, UKM, Bangi, Selangor 43600, Malaysia

[2] Faculty of Science and Technology, Universiti Sains Islam Malaysia, Nilai, Negeri Sembilan 71800, Malaysia

increased its binding affinity to the MrNV capsid protein [11]. A conserved stem-loop has been observed in the truncated aptamer compared to the full-length APT-MrNV-CP-1, suggesting its crucial role in aptamer-protein binding interactions. Although the experimental studies have confirmed the binding potential of the truncated aptamer, the structural and dynamic interactions between the aptamer and the different oligomeric forms of the viral capsid protein remain unexplored. Therefore, understanding the binding dynamics and mechanisms of the aptamer-capsid protein interactions is critical for optimizing the aptamer's functionality and therapeutic potential.

In this study, computational approach utilizing molecular dynamics simulations was employed to investigate the binding interactions between the truncated aptamer and different oligomeric forms of the MrNV capsid protein. MD simulations provide predictive insights into the structural and dynamic behavior of aptamer-protein interactions at the atomic level [12, 13]. The systems were simulated over a 1000 ns timescale to compare the biophysical properties of the aptamer-protein complexes. These findings offer a deeper understanding of how the oligomeric form of the viral capsid protein affects the aptamer recognition and binding affinity, with potential implications for the rational design of aptamer-based antiviral therapeutics and the development of effective viral detection strategies.

Methodology

Ligand preparation and molecular docking

The secondary structure of the truncated aptamer was predicted using UNAFold webserver (http://www.unafold.org/mfold/applications/dna-folding-form.php). Based on this secondary structure, the three-dimensional structure of the truncated aptamer was then constructed using 3dRNA web tool (http://biophy.hust.edu.cn/new/3dRNA). Prior to molecular docking, the structure was refined by adding hydrogen atoms. Molecular docking was performed using HDOCK (http://hdock.phys.hust.edu.cn/), where the refined 3D aptamer structure was used as the ligand and the MrNV capsid protein (PDB ID: 6H2B) was designated as the target. The aptamer-viral capsid protein complex with the most stable predicted binding interactions based on the docking energy score, was selected for subsequent molecular dynamics simulations.

System preparation for molecular dynamics simulations

Molecular dynamics simulations were performed using GROMACS [14, 15], with the CHARMM36 force field applied to simulate molecular interactions [16]. The initial atomic coordinates obtained from molecular docking were further refined using CHARMM-GUI [17], and the system was neutralized with counterions as needed. The final solvated and neutralized systems contained approximately 221,984 atoms for the monomeric MrNV capsid protein-aptamer complex and 606,104 atoms for the trimeric MrNV capsid protein-aptamer complex, including the solute (protein and aptamer), water molecules, and counterions. Energy minimization was performed using the steepest descent algorithm for 50,000 iterations to ensure steric conflict resolution and structural stability [18]. During this phase, no temperature or pressure coupling was applied. Subsequently, the system underwent equilibration in two successive phases: NVT equilibration (constant Number, Volume, and Temperature), where the system was equilibrated at 300 K using the velocity-rescale (v-scale) thermostat to stabilize temperature [19]; and NPT equilibration (constant Number, Pressure, and Temperature), where the system was equilibrated at 1 bar utilizing the Berendsen barostat to ensure proper system density and pressure stabilization. Each equilibration phase was performed with a time step of 1 fs (0.001 ps) for 125,000 steps to allow solvent molecules to reach equilibrium.

Production molecular dynamics simulations

Following equilibration, the system was subjected to production molecular dynamics simulation under NPT ensemble conditions for a duration of 1 μs (1,000 ns), with a time step of 2 femtoseconds (0.002 picoseconds). The v-rescale thermostat was applied to maintain a stable temperature, while the C-rescale barostat was applied to regulate pressure at 1 bar. The Particle Mesh Ewald (PME) method was used to compute long-range electrostatic interactions, while van der Waals interactions were calculated with a 1.2 nm cutoff. The LINCS algorithm was employed to constrain bond lengths, facilitating the utilization of a bigger time step in the simulation.

Binding free energy calculations using MM/PBSA approach

The binding free energy of the aptamer-MrNV capsid protein complex was estimated using the Molecular Mechanics Poisson-Boltzmann Surface Area (MM/PBSA) method, implemented via gmx_MMPBSA [20]. A total of 1000

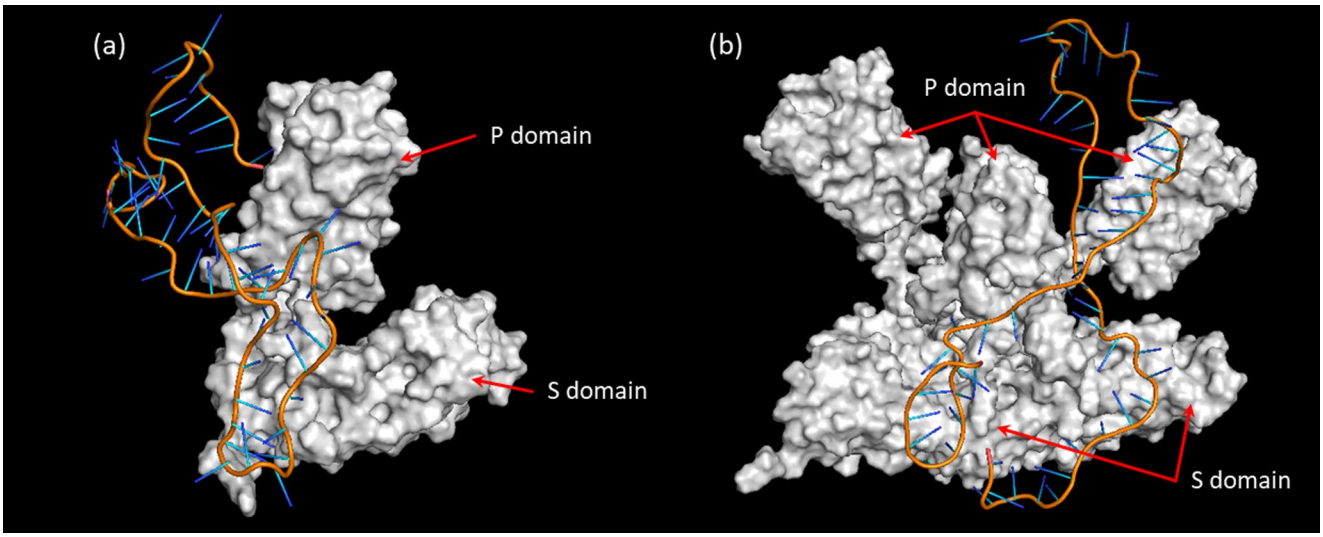

Fig. 1 Molecular docking of the truncated aptamer with (**a**) monomeric and (**b**) trimeric MrNV capsid proteins. The aptamer exhibited binding that extends across the protruding (P) domain to the shell (S) domain, suggesting a continuous interaction spanning both domains of the viral capsid protein

Table 1 Molecular docking of the TrAptm-1 aptamer with monomeric and trimeric MrNV capsid proteins

	Monomeric MrNV capsid protein	Trimeric MrNV capsid protein
Docking Score	-314.49	-308.93
Confidence Score	0.9641	0.9600
Ligand RMSD (Å)	0.21	66.01

snapshots were extracted at 1 ns intervals from the 1000 ns production MD trajectory to ensure statistically robust and representative sampling. Energy calculations were performed using the FF99SB force field, and solvation effects were modeled using the Poisson–Boltzmann (PB) approach. The solute and solvent dielectric constants were set to 1.0 and 80.0, respectively. Nonpolar solvation contributions were computed using a surface tension model with surften = 0.0072 and surfresc = 0.00. A single-trajectory approach was used for consistency across the complex, protein, and aptamer components. The binding free energy was calculated using the following equation:

$$\Delta G_{binding} = G_{complex} - (G_{receptor} + G_{ligand})$$

Where:

$G_{complex}$ = free energy of the bound aptamer-protein complex;

$G_{receptor}$ = free energy of the unbound viral capsid protein;

G_{ligand} = free energy of the unbound aptamer.

Further decomposition of the binding free energy was performed to evaluate contributions from molecular mechanics and solvation effects:

$$\Delta G_{binding} = (\Delta E_{vdW} + \Delta E_{elec}) + (\Delta G_{polar} + \Delta G_{nonpolar})$$

Where:

ΔE_{vdW} = van der Waals interaction energy;

ΔE_{elec} = electrostatic interaction energy;

ΔG_{polar} = polar solvation free energy;

$\Delta G_{nonpolar}$ = non-polar solvation free energy;

Results

Molecular docking analysis of the TrAptm-1 aptamer with monomeric and trimeric MrNV capsid proteins

Molecular docking was performed to predict the best docked position of the TrAptm-1 aptamer with the monomeric and trimeric MrNV capsid proteins. The docking results revealed that the aptamer interacts with both the protruding (P) domain and the shell (S) domain of the viral capsid protein in both structural forms (Fig. 1).

The aptamer demonstrated a slightly stronger binding affinity for the monomeric capsid protein, as indicated by the more negative docking score (-314.49) compared to the trimeric capsid protein (-308.93) (Table 1). Both complexes exhibited high confidence scores (> 0.7), implying a strong likelihood of binding. However, the higher ligand RMSD in the trimeric complex indicates greater structural deviation of the aptamer in the docked model relative to its input conformation. Both complexes were subsequently subjected to a 1000-ns molecular dynamics simulation to evaluate their structural stability and binding dynamics.

Molecular dynamics simulation of the TrAptm-1 aptamer with monomeric and trimeric MrNV capsid proteins

Molecular dynamics simulations of the TrAptm-1 aptamer in complex with monomeric and trimeric capsid proteins were analyzed using Root Mean Square Deviation (RMSD) and Root Mean Square Deviation (RMSF) to examine the structural stability and conformational dynamics over the 1000 ns simulation. The aptamer-trimeric capsid protein complex showed higher RMSD values (approximately 1.2–1.5 nm) compared to the aptamer-monomeric capsid protein complex (approximately 0.5–0.7 nm) (Fig. 2a), indicating higher structural flexibility. Notably, the RMSD of the aptamer-trimeric capsid protein complex fluctuated significantly during the initial 0 to 300 ns before stabilizing beyond 300 ns, suggesting early structural adjustments before reaching equilibrium. In contrast, the aptamer-monomeric capsid protein complex maintained a relatively stable RMSD throughout the simulation. Similarly, the aptamer-trimeric capsid protein complex exhibited higher RMSF values than the aptamer-monomeric capsid protein complex (Fig. 2b), indicating greater local flexibility in specific residue regions - residue 250–371 (P domain). In contrast, the lower RMSF observed in the aptamer-monomeric capsid protein complex reflecting a more rigid and stable structure.

The radius of gyration (Rg) analysis was conducted to evaluate the overall compactness of the aptamer-monomeric and aptamer-trimeric capsid protein complexes throughout the simulation. The results indicate that the aptamer-monomeric capsid protein complex initially adopts a more expanded conformation (0 to 50 ns) before gradually

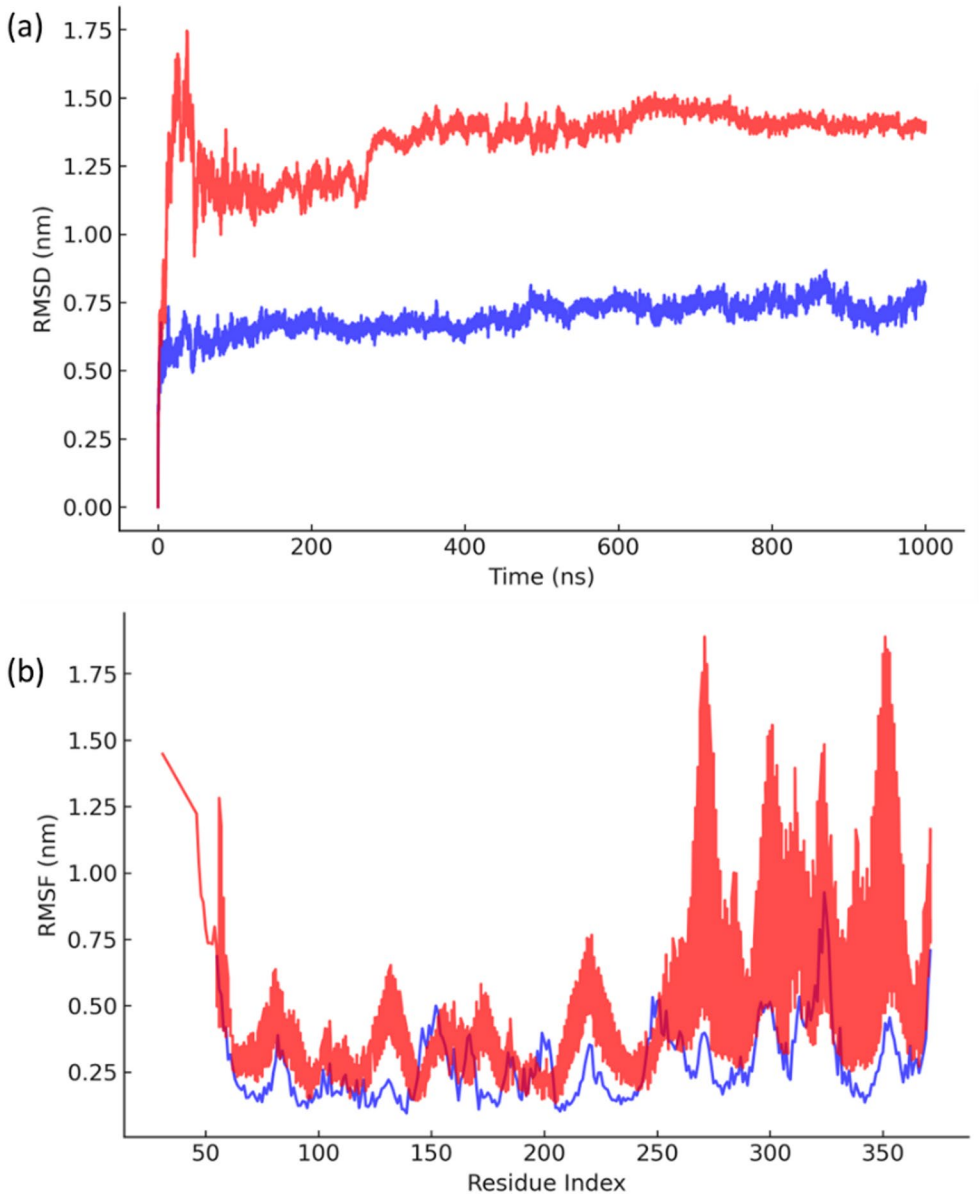

Fig. 2 Root Mean Square Deviation (RMSD) (**a**) and Root Mean Square Fluctuation (RMSF) (**b**) of the TrAptm-1 aptamer in complex with monomeric (blue line) and trimeric (red line) capsid protein

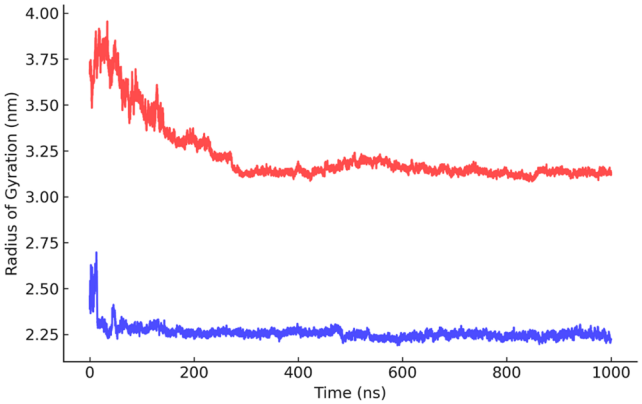

Fig. 3 Radius of gyration (Rg) of the TrAptm-1 aptamer in complex with monomeric (blue line) and trimeric (red line) capsid protein over a 1000 ns simulation

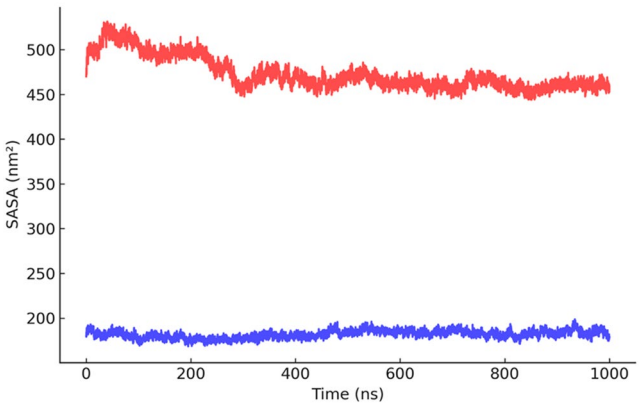

Fig. 4 Comparison of Solvent Accessible Surface Area (SASA) for the TrAptm-1 aptamer in complex with monomeric capsid protein (blue line) and trimeric capsid protein (red line) over 1000 ns simulation time

stabilizing (Fig. 3). In contrast, the aptamer-trimeric CP complex maintains a higher Rg and only stabilizes after approximately 250 ns, reflecting a more extended and dynamic structural arrangement over a prolonged period before achieving stability.

The binding interactions between the TrAptm-1 aptamer and the monomeric and trimeric forms of the MrNV capsid protein were assessed using Solvent-Accessible Surface Area (SASA) analysis. The solvent-exposed surface area of the complexes was measured to identify interaction sites by evaluating changes in accessibility upon binding. A lower SASA was recorded for the aptamer-monomeric capsid protein complex (approximately 150–200 nm^2) (Fig. 4), suggesting a more compact interaction with reduced solvent exposure. In contrast, the aptamer-trimeric capsid protein complex showed a higher SASA (approximately 450–500 nm^2), likely due to the larger size of the trimeric capsid protein. Despite this difference, both complexes maintained relatively stable SASA values throughout the 1000 ns

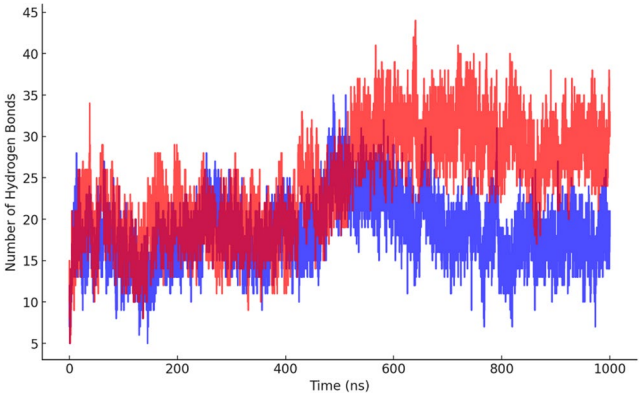

Fig. 5 Hydrogen bond analysis of the TrAptm-1 aptamer-capsid protein complexes. The number of hydrogen bonds formed between the aptamer and monomeric capsid protein (blue line) and trimeric capsid protein (red line) were monitored throughout the 1000 ns simulation

simulation, indicating no significant unfolding or dissociation. However, higher SASA fluctuations were observed in the aptamer-trimeric capsid protein complex during the initial 0–300 ns before stabilizing beyond 300 ns, suggesting early structural adjustments before reaching equilibrium.

The number of hydrogen bonds between the TrAptm-1 aptamer and the trimeric capsid protein increased from 10 to 30 to 25–40 after 500 ns of simulation (Fig. 5), suggesting that the aptamer adapted to a more complex binding interface and achieved stabilization. In contrast, the hydrogen bonds formed between the TrAptm-1 aptamer and the monomeric capsid protein remain relatively stable (~15–30) throughout the simulation, indicating a more consistent interaction pattern.

The structural variations were analyzed using Principal Component Analysis (PCA) to examine the conformational changes and overall flexibility of both the complexes (Fig. 6). The PCA results showed a relatively smaller spread of data points along PC1 and PC2 for the TrAptm-1 aptamer in complex with the monomeric capsid protein (Fig. 6a) compared to its complex with the trimeric capsid protein (Fig. 6b). This suggests that the aptamer-monomer complex exhibited restricted movement, resulting in fewer conformational variations. In contrast, the aptamer-trimeric capsid protein complex showed greater conformational fluctuations, as indicated by the dispersed data points in the PCA plot. This implies a more diverse range of binding interactions and overall structural rearrangements in aptamer-trimeric capsid protein complex.

Structural snapshots at 10 ns, 100 ns, 500 ns, and 900 ns were captured to visualize the progressive conformational changes in the TrApt-1 aptamer and its interactions with both the monomeric (Fig. 7) and trimeric (Fig. 8) capsid proteins. Over the selected trajectory time points, significant structural rearrangements were observed in the aptamer,

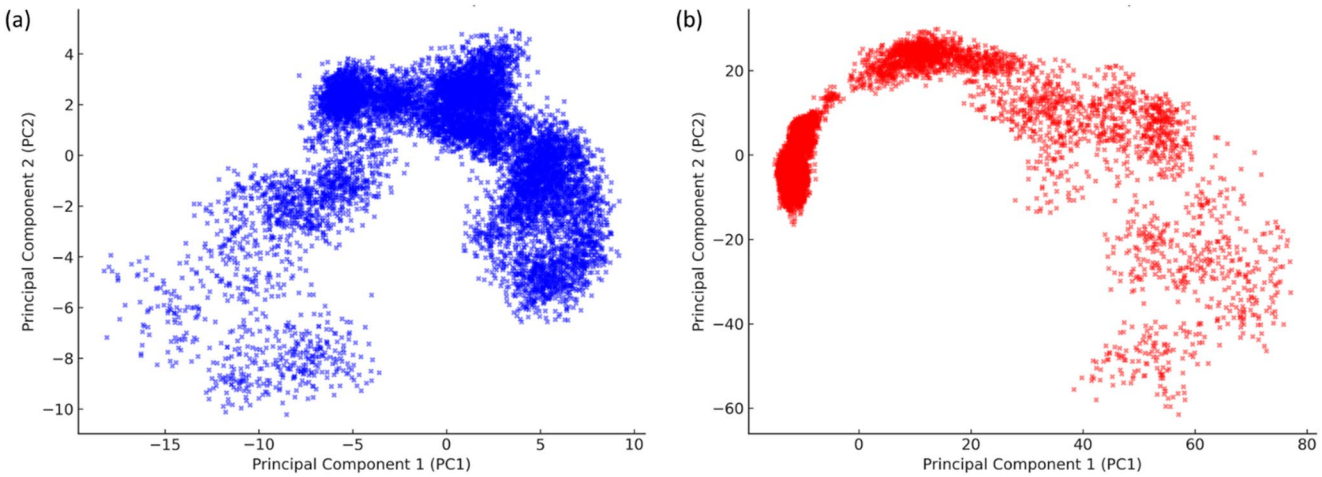

Fig. 6 Principal Component Analysis (PCA) scatter plots illustrating the structural variations of the TrAptm-1 aptamer in complex with (**a**) monomeric capsid protein and (**b**) trimeric capsid protein. The PCA plots highlight the conformational dynamics and overall flexibility of the aptamer-protein interactions, with a broader distribution of the plots indicating greater structural adaptability in the binding interactions

suggesting a potential optimization of its binding interface with the capsid proteins.

Notably, the protruding (P) domains, which were distinctly separated at an earlier time point (Figs. 8a and 9 ns; green and yellow P domains), progressively shifted closer together over time (Figs. 8a and 100 ns, 500 ns, 900 ns). Additionally, the third P domain (beige) shifted toward the shell (S) domain (Fig. 8c). These structural rearrangements suggested increased interactions between the domains, indicating surface contact that may contribute to the overall stabilization of the aptamer-protein complex. Further analysis of hydrogen bond (H-bond) interactions between the domains revealed the formation of multiple H-bonds, reinforcing the closer positioning of these domains (Fig. 10). A similar shift of the P domain toward the S domain was also observed in the monomeric capsid protein upon aptamer binding, with multiple H-bond interactions forming as early as 100 ns (Fig. 9).

The binding free energy components for the interaction between the TrAptm-1 aptamer and both monomeric and trimeric capsid proteins were computed using the MMPBSA approach (Table 2). The binding free energy ($\Delta G_{binding}$) was lower for the aptamer-trimeric capsid protein complex (-153.95 kcal/mol) compared to the aptamer-monomeric capsid protein complex (-120.77 kcal/mol), indicating a stronger binding affinity for the trimeric capsid protein. The aptamer-trimeric capsid protein complex exhibited more favorable van der Waals (VDWAALS) and polar solvation energy (EGB) contributions. In contrast, the non-polar solvation energy (ESURF) had a minimal contribution on stabilizing the complex. These findings showed that while the TrAptm-1 aptamer can bind to both the monomeric and trimeric MrNV capsid proteins, it exhibited greater stability and stronger interactions with the trimeric form of the capsid protein.

Discussion

The present study expands on previously validated aptamer-based detection platform targeting the *Macrobrachium rosenbergii* nodavirus (MrNV) capsid protein. In earlier studies, high-affinity aptamers capable of specific binding to the MrNV capsid protein were successfully identified and characterized, demonstrated potential for aptamer-based biosensing applications [10]. Furthermore, strategic truncation of the lead aptamer candidate was found to enhance its binding affinity, as confirmed through in vitro binding assay [11]. These findings established a solid experimental foundation for the current computational investigation. In this study, the aptamer's secondary structure was first predicted using UNAFold, and subsequently used to construct the 3D structure using 3dRNA, a widely-adopted and well-validated tool for RNA structural modeling. This two-step approach was employed to mitigate the inherent challenges associated with RNA 3D structure prediction, which remain difficult due to the molecule's high conformational flexibility. Notably, 3dRNA has demonstrated strong performance in benchmark assessments and is capable of generating biologically plausible models guided by experimentally informed secondary structures.

Long-timescale molecular dynamics (MD) simulations (1 µs) was employed in this study to explore the conformational dynamics and domain-specific interactions between the truncated aptamer, TrAptm-1 and the MrNV capsid protein. These atomistic-level insights are not easily accessible through experimental methods alone but are critical

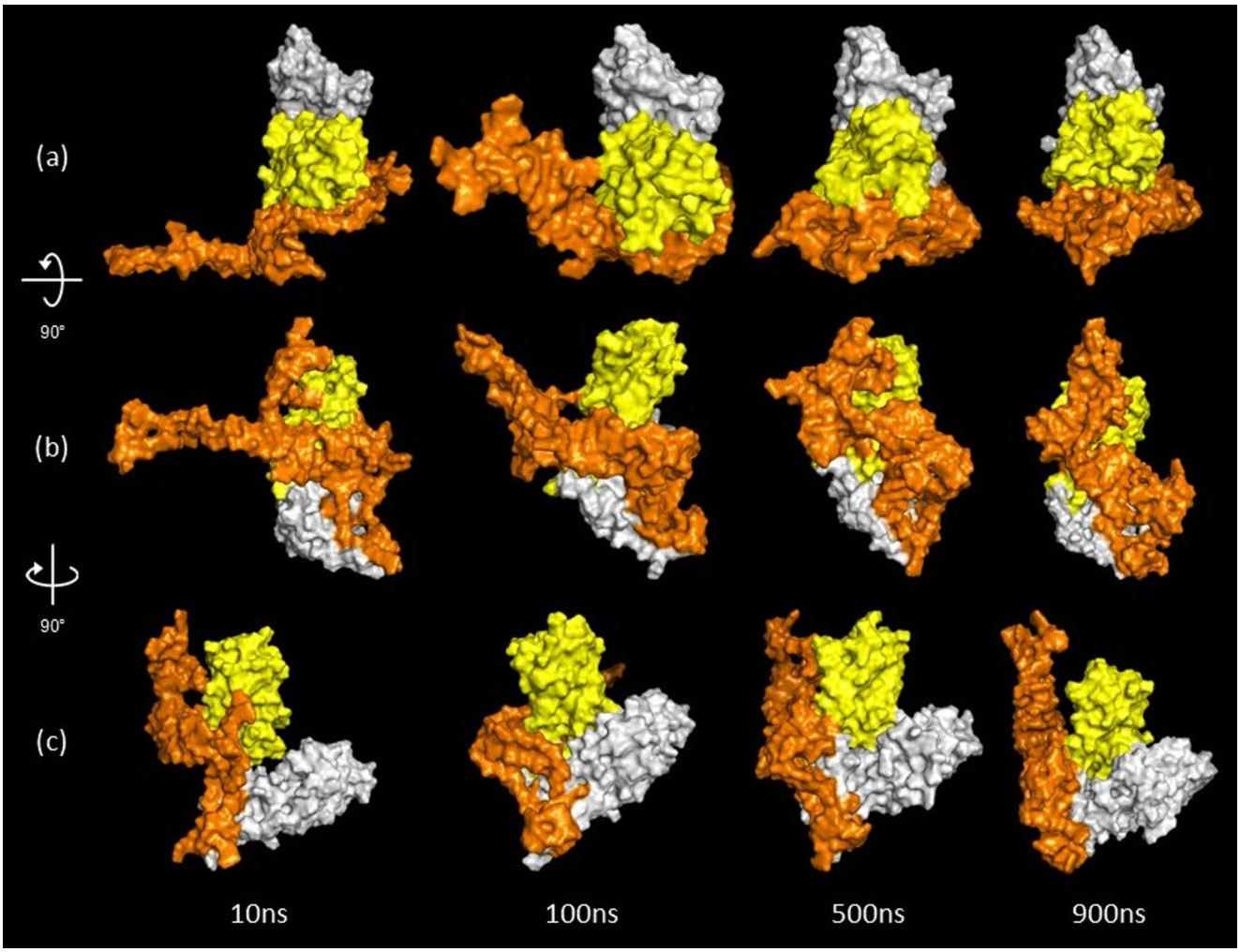

Fig. 7 Conformational dynamics of the monomeric capsid protein and TrApt-1 aptamer during molecular dynamics simulation. Structural snapshots at 10 ns, 100 ns, 500 ns, and 900 ns illustrate the progressive changes in the aptamer-protein complex. The viral capsid protein is shown in surface representation with different domain colored as follows: grey for the shell (S) domain; and yellow for the protruding (P) domain. The TrApt-1 aptamer is shown in orange. Structural rearrangements highlighted the dynamic interactions and stabilization of the complex over the 1000 ns simulation. (**a**) capsid protein viewed along the 3-fold axis; (**b**) lateral view of the protein rotated 90° along the *x*-axis from (**a**); (**c**) lateral view of the protein rotated 90° along the *y*-axis from (**b**)

for understanding the mechanistic basis of aptamer binding and its impact on capsid structural modulation. While MD simulations inherently rely on force field approximations and are subjected to limitations in temporal sampling, the reliability of the modeled interaction is strengthened by prior experimental confirmation of aptamer-capsid binding. Structural integrity and conformational behavior of both monomeric and trimeric forms of the MrNV capsid protein upon TrAptm-1 aptamer binding were examined over a 1 µs simulation timeframe. The RMSD analysis demonstrated that the aptamer-bound trimeric capsid protein exhibited greater structural deviations compared to the aptamer-monomeric capsid protein complex (Fig. 2a), possibly due to the domains flexibility and movements. This was confirmed in RMSF analysis that highlighted the significant fluctuations in the protruding (P) domain (residue 250–371) (Fig. 2b). Notably, the broader trace of the red line in Fig. 2b reflects the combined variability of three independent P-domains present in the trimeric assembly, each undergoing distinct conformational motions during the simulation. This multiplicity resulted in a wider distribution of fluctuations. These domain-specific flexibilities may contribute to the conformational adaptability of the capsid protein upon aptamer binding. Additionally, the radius of gyration analysis showed a progressive structural compaction in the aptamer-bound trimeric capsid protein complex that stabilized beyond 300 ns (Fig. 3), suggesting a dynamic structural changes of the aptamer-trimeric capsid protein complex. Similar was found in Principal Component Analysis that showed greater conformational fluctuations of the

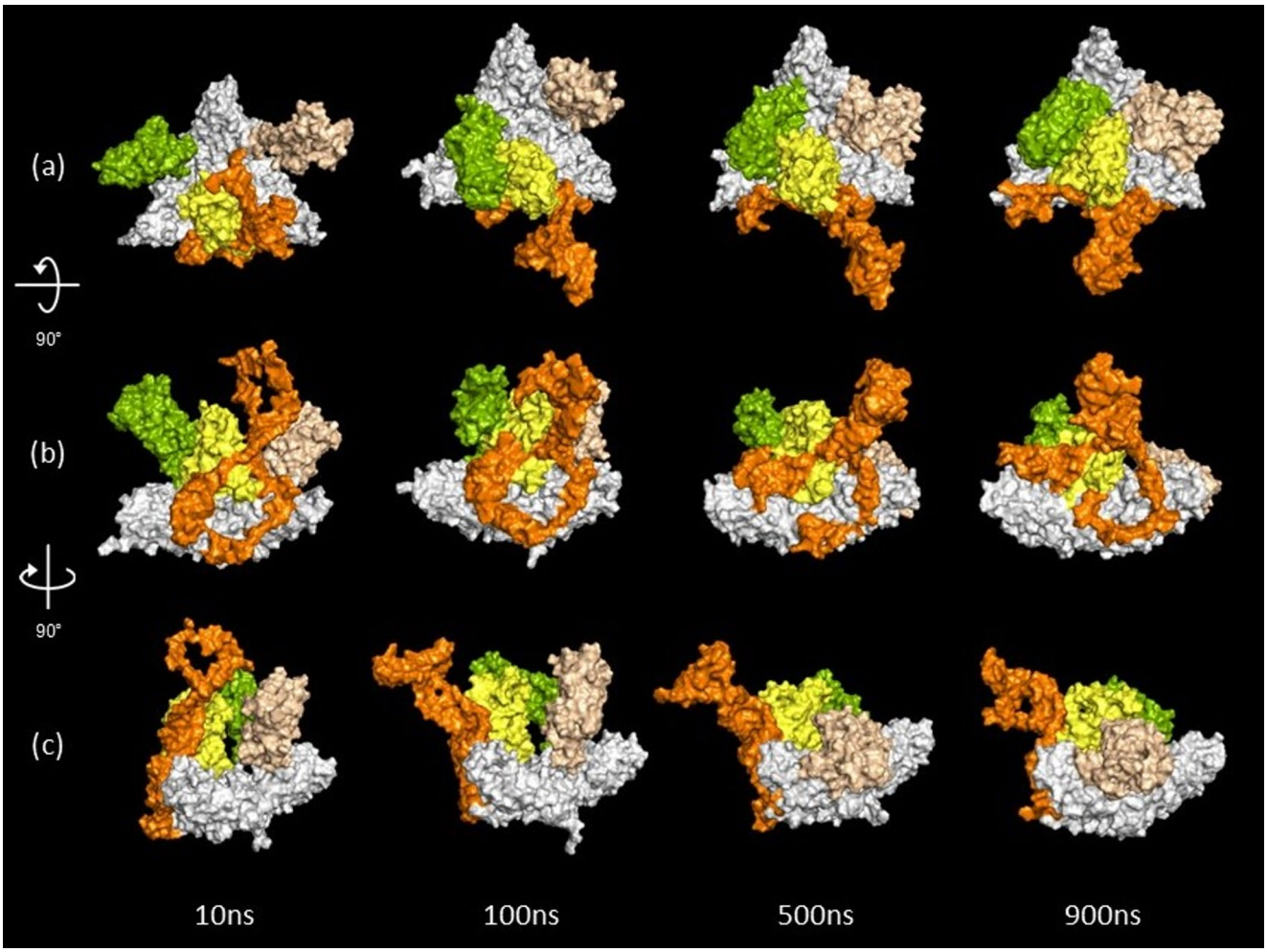

Fig. 8 Conformational dynamics of the trimeric capsid protein and TrApt-1 aptamer during molecular dynamics simulation. Structural snapshots at 10 ns, 100 ns, 500 ns, and 900 ns illustrate the progressive changes in the aptamer-protein complex. The viral capsid protein is shown in surface representation with different domain colored as follows: grey for the shell (S) domain; and beige, yellow and green for the protruding (P) domains of chain A, B, and C, respectively. The TrApt-1 aptamer is shown in orange. Structural rearrangements highlighted the dynamic interactions and stabilization of the complex over the 1000 ns simulation. (**a**) T = 3 capsid protein assembly viewed along the 3-fold axis; (**b**) lateral view of the trimeric capsid protein rotated 90° along the *x*-axis from (**a**); (**c**) lateral view of the trimeric capsid protein rotated 90° along the *y*-axis from (**b**)

complex indicated by the dispersed data points in the PCA plot (Fig. 6). The solvent accessible surface area (SASA) analysis also indicated progressive structural compaction in the aptamer-bound trimeric capsid protein complex, as evidenced by a noticeable decrease in SASA within the initial 200–300 ns. This reduction suggests decreased solvent exposure of the overall complex, which may be associated with stable binding interactions. Additionally, the number of hydrogen bonds increased and stabilized after ~500 ns, indicated a strengthened interaction between the aptamer and the trimeric capsid protein over time, further supporting stable and persistent molecular interactions. This stable binding affinity is a crucial prerequisite for the development of diagnostic tools for viral capsid proteins detection. Aptamer-based diagnostic strategies have been developed for several other viral diseases, such as largemouth bass virus [21], Zika virus [22–24], dengue virus [25] etc. A preliminary assay utilizing the TrAptm-1 aptamer as a sensor in both enzyme-linked aptamer assay (ELAA) and gold nanoparticle-based aptasensor assay had demonstrated consistent results in detecting the viral capsid protein in the cell lysate of MrNV-infected prawns [11].

Structural snapshots of the complex at 10 ns, 100 ns, 500 ns, and 900 ns were obtained and analyzed to correlate the observed biophysical changes from MD simulations with structural rearrangements in the 3D conformation of the complex. Visualization of these snapshots revealed that the observed biophysical changes were likely due to the dynamic interactions between the P-P and P-S domains (Figs. 8 and 10), where progressive conformational changes

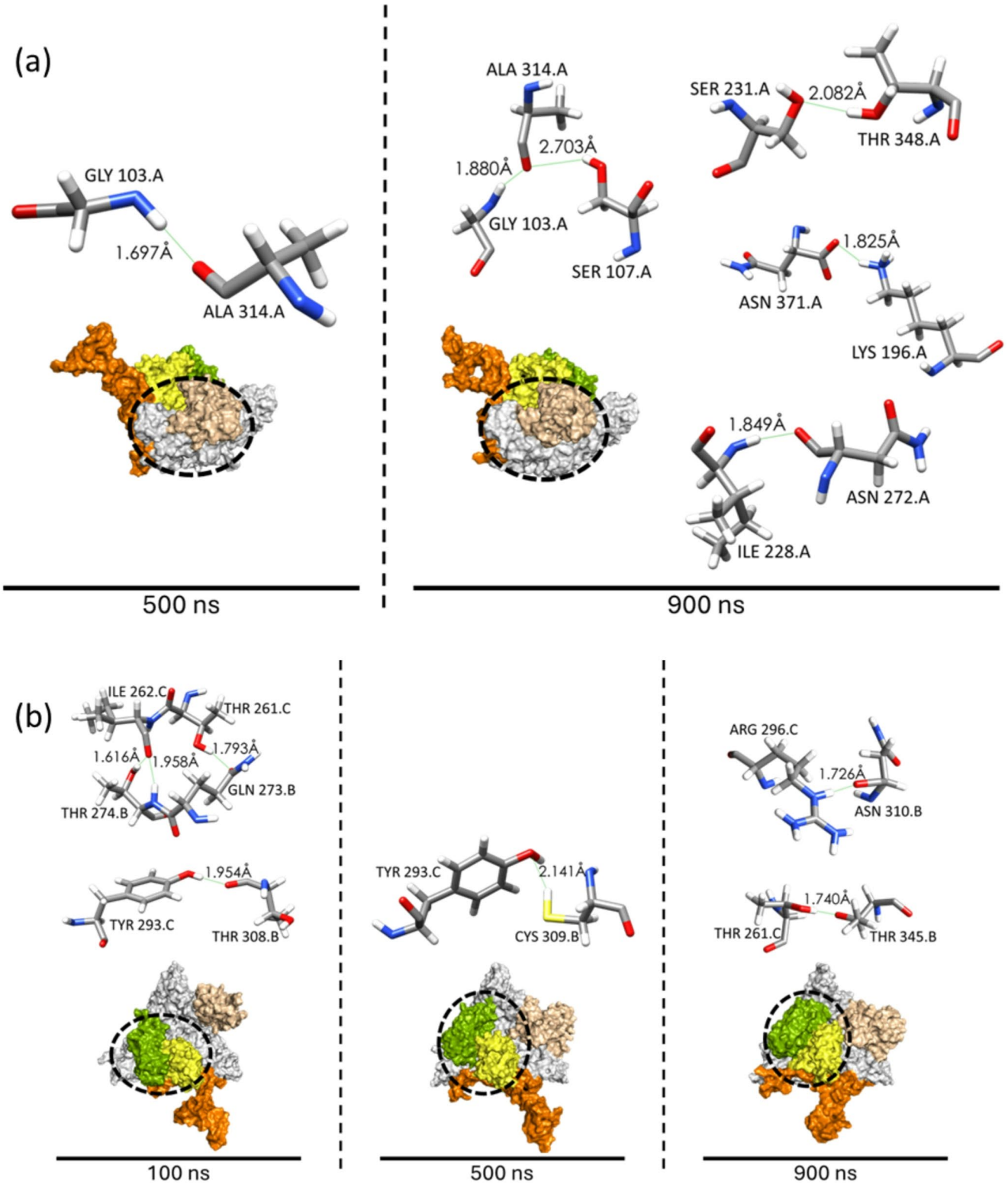

Fig. 9 Hydrogen bond (H-bond) analysis of the trimeric capsid protein upon aptamer binding. (**a**) H-bond interactions between the protruding (P) domain (beige) and the shell (S) domain of chain A. (**b**) H-bond interactions between the P domains of chain B (yellow) and chain C (green)

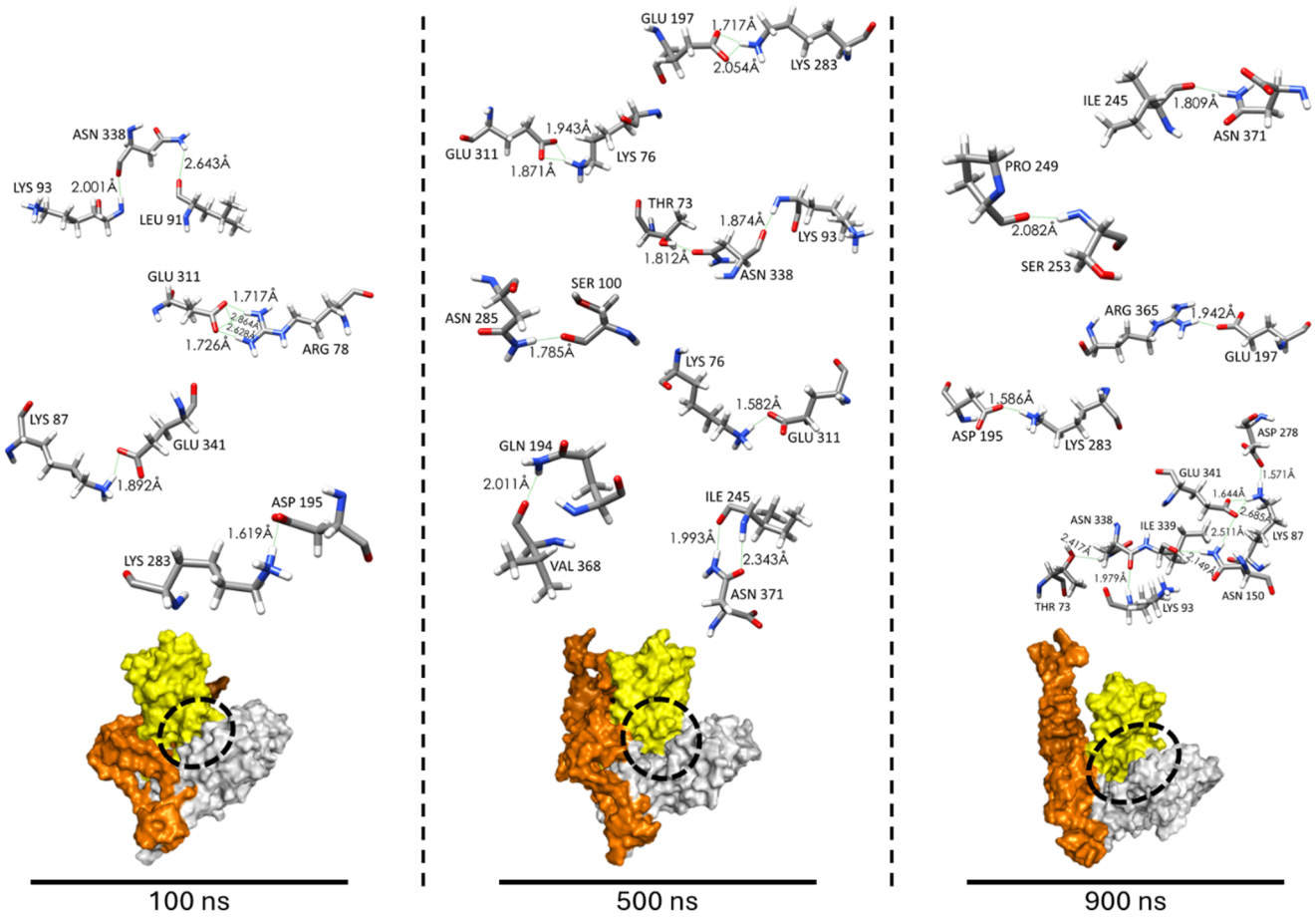

Fig. 10 Hydrogen bond (H-bond) analysis between the P domain and S domain of the monomeric MrNV capsid protein upon aptamer binding

Table 2 Molecular Mechanics/Poisson-Boltzmann surface area (MMPBSA) binding free energy analysis of TrAptm-1 aptamer in complex with monomeric and trimeric capsid proteins. All energy values are presented as mean ± standard error of the mean (SEM) in kcal/mol

Energy Component	Monomeric MrNV-CP, kcal/mol	Trimeric MrNV-CP, kcal/mol
Van der Waals Energy, VDWAALS	-117.13 ± 2.42	-145.35 ± 6.15
Electrostatic Energy, EEL	214.27 ± 4.24	438.5 ± 6.09
Generalized Born Solvation Energy, EGB	-204.33 ± 4.05	-429.74 ± 6.09
Non-Polar Solvation Energy, ESURF	-13.59 ± 0.22	-17.37 ± 0.74
Gas Phase Energy, GGAS	97.14 ± 4.84	293.15 ± 11.23
Solvation Energy, GSOLV	-217.91 ± 4.12	-447.11 ± 5.56
Binding Free Energy, $\Delta G_{binding}$	-120.77 ± 2.46	-153.95 ± 6.74

and structural rearrangements were recorded. The S domain forms the main capsid shell, providing stability and encapsidates the viral RNA genome, while the P domain extends outward, typically involves in the host receptor recognition and interaction, playing a crucial role in viral attachment and entry. The structural rearrangements and conformational changes observed in both the monomeric and trimeric forms of the capsid protein upon aptamer binding are particularly important for the development of therapeutic aptamers with anti-viral properties. Previous studies have reported that ligand-induced subtle but significant rearrangements in the viral capsid protein affect the capsid assembly, contributing to anti-viral effects [26–28]. Current observation that TrAptm-1 aptamer binding induced distinct structural rearrangement in both monomeric and trimeric MrNV capsid proteins, suggesting a potential interference of the capsid protein self-assembly process. The observed structural disruption in current analysis provides a strong foundation for further in-vitro evaluation of the aptamer's anti-viral potential against MrNV. Although the anti-MrNV properties of the TrAptm-1 aptamer have not yet been studied, aptamer-based therapeutic strategies have been reported against several viral pathogens, including largemouth bass virus [3], grouper nervous necrosis virus [29], SARS-CoV-2 [30], and hepatitis C virus [31], demonstrating the broad potential of aptamers as antiviral agents across both aquatic and human viral diseases. Meanwhile, these findings highlighted the importance of longer simulation times to allow the system

to explore biologically relevant conformational states that may play a critical role in both protein and aptamer stability and function. Given that large protein complexes often undergo slow and progressive structural changes, extending the MD simulation beyond microsecond could provide deeper insights into the long-term dynamics of aptamer-protein interactions and their functional implications [32–34].

The MMPBSA binding free energy analysis revealed a higher binding affinity of the TrAptm-1 aptamer for the trimeric capsid protein (-153.95 kcal/mol) compared to the monomeric form (-120.77 kcal/mol). A similar observation was reported, where the aptamer CA15-2 selectively bound to the assembled HIV-1 capsid lattice, but not to its monomeric or hexameric forms [35]. This supported the understanding that aptamer recognition and binding affinity can vary significantly with the oligomeric state of the target protein, consistent with the differences observed between the monomeric and trimeric capsid proteins in this study. While this study demonstrated detailed aptamer-MrNV capsid protein interactions at the atomic-level through MD simulations and MMPBSA binding free energy calculation, certain limitations should be acknowledged. Notably, the binding free energy calculations presented did not include entropic contributions ($-T\Delta S$), which often omitted in MMPBSA analysis due to the high computational cost and potential convergence issues associated with normal mode or quasi-harmonic entropy calculations, especially in large nucleic acid-protein complexes. Thus, the reported binding free energy represented primarily the enthalpic component of the interaction. Although this is a widely accepted approach for comparative binding analysis, it may not fully capture the influence of conformational entropy, particularly relevant for flexible ligands such as aptamers. Nonetheless, the binding of TrAptm-1 to the MrNV capsid protein has been previously validated through in vitro experimental assays [11], providing orthogonal evidence that supports the reliability of the current predicted interaction.

Conclusion

The molecular dynamics simulations and binding energy analyses revealed that the TrAptm-1 aptamer exhibits a higher binding affinity for the trimeric capsid protein, induced conformational changes and structural rearrangements that contributed to an enhanced binding stability. These findings provide insights for the rational design of aptamer-based antiviral strategies and the development of biosensors for MrNV detection in aquaculture.

Acknowledgements This work was supported by the Ministry of Higher Education, Malaysia under the Fundamental Research Grant Scheme, FRGS (Grant number: FRGS/1/2018/STG05/UKM/02/1).

Author contributions Low CF contribution in Conceptualization, Data curation, Funding acquisition, Methodology, Project administration, Resources, Supervision, Validation, Writing – review & editing. Norazli G. contribution in Data curation, Formal analysis, Investigation, Methodology, Resources, Validation, Writing – original draft. Muhamad Arif MJ contribution in Data curation, Methodology, Resources, Supervision, Validation, Writing – review & editing. All authors reviewed the manuscript.

Funding Open access funding provided by The Ministry of Higher Education Malaysia and Universiti Kebangsaan Malaysia.

Data availability No datasets were generated or analysed during the current study.

Declarations

Competing interests The authors declare no competing interests.

References

1. Ganesan H, Ho KL, Mariatulqabtiah AR, Yong CY, Wong CL, Goh ZH et al (2022) Virus-like particles of Macrobrachium rosenbergii nodavirus: particle size and capsid protein assembly domain. Aquaculture 561:738670
2. Chakraborty B, Das S, Gupta A, Xiong Y, TV V, Kizer ME et al (2022) Aptamers for viral detection and Inhibition. ACS Infect Dis 8(4):667–692
3. Yu Q, Li M, Liu M, Huang S, Wang G, Wang T et al (2021) Selection and characterization of SsDNA aptamers targeting large-mouth bass virus infected cells with antiviral activities. Front Microbiol 12:785318
4. Dzuvor CKO, Tettey EL, Danquah MK (2022) Aptamers as promising nanotheranostic tools in the COVID-19 pandemic era. Wiley Interdiscip Rev Nanomed Nanobiotechnol 14(3):e1785
5. Hu C, Yang S, Li S, Liu X, Liu Y, Chen Z et al (2024) Viral aptamer screening and aptamer-based biosensors for virus detection: A review. Int J Biol Macromol. 133935
6. Chong C, Low C (2019) Synthetic antibody: prospects in aquaculture biosecurity. Fish Shellfish Immunol. 86
7. Krüger A, de Jesus Santos AP, de Sá V, Ulrich H, Wrenger C (2021) Aptamer applications in emerging viral diseases. Pharmaceuticals 14(7):622
8. Zhang T, Lu Y, Deng S, Deng R (2021) Aptamers for the diagnosis of infectious diseases. Aptamers Med Appl Diagnosis Ther. 207–238

9. Chen Z, Sun Q, Yang Y, Nie X, Xiang W, Ren Y et al (2024) Aptamer-based diagnostic and therapeutic approaches for animal viruses: A review. Int J Biol Macromol 257:128677
10. Ghadin N, Yusof NAM, Syarul Nataqain B, Raston NHA, Low CF (2024) Selection and characterization of SsDNA aptamer targeting Macrobrachium rosenbergii nodavirus capsid protein: A potential capture agent in gold-nanoparticle-based aptasensor for viral protein detection. J Fish Dis 47(2):1–11
11. Ghadin N, Baharum SN, Ahmad Raston NH, Low C-F (2025) Truncation-Enhanced aptamer binding affinity and its potential as a sensor for Macrobrachium rosenbergii nodavirus detection. J Fish Dis. e14093
12. Cleri F, Lensink MF, Blossey R (2021) DNA aptamers block the receptor binding domain at the Spike protein of SARS-CoV-2. Front Mol Biosci 8:713003
13. Sun M, Liu S, Wei X, Wan S, Huang M, Song T et al (2021) Aptamer blocking strategy inhibits SARS-CoV-2 virus infection. Angew Chemie Int Ed 60(18):10266–10272
14. Abraham MJ, Murtola T, Schulz R, Páll S, Smith JC, Hess B et al (2015) GROMACS: high performance molecular simulations through multi-level parallelism from laptops to supercomputers. SoftwareX 1:19–25
15. Van Der Spoel D, Lindahl E, Hess B, Groenhof G, Mark AE, Berendsen HJC (2005) GROMACS: fast, flexible, and free. J Comput Chem 26(16):1701–1718
16. Huang J, MacKerell AD Jr (2013) CHARMM36 all-atom additive protein force field: validation based on comparison to NMR data. J Comput Chem 34(25):2135–2145
17. Jo S, Kim T, Iyer VG, Im W (2008) CHARMM-GUI: a web-based graphical user interface for CHARMM. J Comput Chem 29(11):1859–1865
18. Hess B, Kutzner C, Van Der Spoel D, Lindahl E (2008) GROMACS 4: algorithms for highly efficient, load-balanced, and scalable molecular simulation. J Chem Theory Comput 4(3):435–447
19. Bussi G, Donadio D, Parrinello M (2007) Canonical sampling through velocity rescaling. J Chem Phys;126(1)
20. Valdés-Tresanco MS, Valdés-Tresanco ME, Valiente PA, Moreno E (2021) gmx_MMPBSA: a new tool to perform end-state free energy calculations with GROMACS. J Chem Theory Comput 17(10):6281–6291
21. Zhang X, Zhang Z, Li J, Huang X, Wei J, Yang J et al (2022) A novel sandwich ELASA based on aptamer for detection of large-mouth bass virus (LMBV). Viruses 14(5):1–10
22. Bosak A, Saraf N, Willenberg A, Kwan MWC, Alto BW, Jackson GW et al (2019) Aptamer-gold nanoparticle conjugates for the colorimetric detection of arboviruses and vector mosquito species. RSC Adv 9(41):23752–23763
23. Nguyen ATV, Duong BT, Park H, Yeo S-J (2022) Development of a peptide aptamer pair-linked rapid fluorescent diagnostic system for Zika virus detection. Biosens Bioelectron 197:113768
24. Park G, Lee M, Kang J, Park C, Min J, Lee T (2022) Selection of DNA aptamer and its application as an electrical biosensor for Zika virus detection in human serum. Nano Converg 9(1):41
25. Thevendran R, Rogini S, Leighton G, Mutombwera A, Shigdar S, Tang T-H et al (2023) The diagnostic potential of RNA aptamers against the NS1 protein of dengue virus serotype 2. Biology (Basel) 12(5):722
26. Schlicksup CJ, Wang JC-Y, Francis S, Venkatakrishnan B, Turner WW, VanNieuwenhze M et al (2018) Hepatitis B virus core protein allosteric modulators can distort and disrupt intact capsids. Elife 7:e31473
27. Valiente L, López-Argüello S, Rodr\'\iguez-Huete A, Valbuena A, Mateu MG (2022) Molecular determinants of human rhinovirus infection, assembly, and conformational stability at capsid protein interfaces. J Virol 96(23):e00840–e00822
28. Kant R, Lee L-S, Patterson A, Gibes N, Venkatakrishnan B, Zlotnick A et al (2024) Small molecule assembly agonist alters the dynamics of hepatitis B virus core protein dimer and capsid. J Am Chem Soc 146(42):28856–28865
29. Zhou L, Li P, Yang M, Yu Y, Huang Y, Wei J et al (2016) Generation and characterization of novel DNA aptamers against coat protein of grouper nervous necrosis virus (GNNV) with antiviral activities and delivery potential in grouper cells. Antiviral Res 129:104–114
30. Sun M, Liu S, Song T, Chen F, Zhang J, Huang J et al (2021) Spherical neutralizing aptamer inhibits SARS-CoV-2 infection and suppresses mutational escape. J Am Chem Soc 143(51):21541–21548
31. Torres-Vázquez B, de Lucas AM, Garc\'\ia-Crespo C, Garc\'\ia-Mart\'\in JA, Fragoso A, Fernández-Algar M et al (2022) In vitro selection of high affinity DNA and RNA aptamers that detect hepatitis C virus core protein of genotypes 1 to 4 and inhibit virus production in cell culture. J Mol Biol 167501
32. Bowman GR (2016) Accurately modeling nanosecond protein dynamics requires at least microseconds of simulation. J Comput Chem 37(6):558–566
33. Selvaraj C, Panwar U, Dinesh DC, Boura E, Singh P, Dubey VK et al (2021) Microsecond MD simulation and multiple-conformation virtual screening to identify potential anti-COVID-19 inhibitors against SARS-CoV-2 main protease. Front Chem 8:595273
34. Kumar P, Bhardwaj T, Kumar A, Garg N, Giri R (2022) One microsecond MD simulations of the SARS-CoV-2 main protease and hydroxychloroquine complex reveal the intricate nature of binding. J Biomol Struct Dyn 40(21):10763–10770
35. Gruenke PR, Aneja R, Welbourn S, Ukah OB, Sarafianos SG, Burke DH et al (2022) Selection and identification of an RNA aptamer that specifically binds the HIV-1 capsid lattice and inhibits viral replication. Nucleic Acids Res 50(3):1701–1717